Combination inhibition of PI3K and mTORC1 yields durable remissions in mice bearing orthotopic patient-derived xenografts of HER2-positive breast cancer brain metastases

Jing Ni[1,2,11], Shakti H Ramkissoon[3,4,11], Shaozhen Xie[1,2,11], Shom Goel[1,3], Daniel G Stover[3], Hanbing Guo[1,2], Victor Luu[1,2], Eugenio Marco[5], Lori A Ramkissoon[3], Yun Jee Kang[3], Marika Hayashi[3], Quang-De Nguyen[6], Azra H Ligon[4], Rose Du[7], Elizabeth B Claus[7,8], Brian M Alexander[9,10], Guo-Cheng Yuan[5], Zhigang C Wang[1,3], J Dirk Iglehart[1,3], Ian E Krop[3], Thomas M Roberts[1,2], Eric P Winer[3,12], Nancy U Lin[3], Keith L Ligon[3,4] & Jean J Zhao[1,2,12]

Brain metastases represent the greatest clinical challenge in treating HER2-positive breast cancer. We report the development of orthotopic patient-derived xenografts (PDXs) of HER2-expressing breast cancer brain metastases (BCBM), and their use for the identification of targeted combination therapies. Combined inhibition of PI3K and mTOR resulted in durable tumor regressions in three of five PDXs, and therapeutic response was correlated with a reduction in the phosphorylation of 4EBP1, an mTORC1 effector. The two nonresponding PDXs showed hypermutated genomes with enrichment of mutations in DNA-repair genes, which suggests an association of genomic instability with therapeutic resistance. These findings suggest that a biomarker-driven clinical trial of PI3K inhibitor in combination with an mTOR inhibitor should be conducted for patients with HER2-positive BCBM.

To develop therapeutic strategies for HER2-positive BCBM, we established a panel of orthotopic PDXs (**Fig. 1a**). Fresh BCBMs from two patients, Dana-Farber Brain Metastasis (DF-BM)354 and DF-BM355, were grafted directly into the brains of SCID mice with a median survival of roughly 2–3 months (**Supplementary Fig. 1**). The PDXs resembled the parental BCBMs histologically, as well in their estrogen receptor (ER), progesterone receptor (PR) and HER2 expression (**Fig. 1b**).

We also verified the expression of epithelial marker cytokeratin 7 (CK7) and the absence of glial markers (GFAP and OLIG2) (**Fig. 1b**). We subsequently established PDXs by using BCBMs from three other patients with HER2-positive BCBM. None of the five PDXs expressed detectable levels of the tumor suppressor protein PTEN (**Fig. 1b** and **Supplementary Table 1**). Of 27 clinical specimens of HER2-positive BCBMs, 67% showed no PTEN staining (**Fig. 1c**), which further confirms that the loss of PTEN is widespread in BCBMs[1,2].

To assess the response of HER2-positive BCBMs to targeted therapy, we treated DF-BM355 PDXs with a HER2 kinase inhibitor lapatinib. DF-BM355 PDXs showed no response to lapatinib, which is consistent with the resistance of the donor's tumor to HER2-directed therapy (**Supplementary Fig. 2a,b**). Because DF-BM355 lacks PTEN—a key regulator of the PI3K pathway—we tested the combination of lapatinib with BKM120, a pan-PI3K inhibitor that penetrates the blood–brain barrier (BBB)[3–5]. Again, no response was observed (**Supplementary Fig. 2a,b**).

To understand the lack of response to combined inhibition with HER2 and PI3K, we assessed tumor PI3K-pathway signaling in response to lapatinib and/or BKM120. Although, as compared to the control, these treatments reduced the phosphorlylation of AKT and S6RP—the downstream effectors of PI3K and mTOR, respectively—we observed little change in p-4EBP1, an mTORC1 effector that mediates translation (**Supplementary Fig. 2c,d**). Even combined HER2 and PI3K inhibition therefore did not completely suppress mTORC1 activity in the DF-BM355 model.

Notably, persistent mTOR activity in breast cancers can mediate resistance to PI3K inhibition, and this can be overcome by inhibition with mTORC1 (ref. 6). However, the brain microenvironment is unique, and brain metastases are notoriously refractory to systemic therapies that are effective against extracranial metastases. In keeping with this, it is not known whether mTOR inhibition might overcome PI3K-inhibitor resistance in BCBMs. To explore this, we combined either lapatinib or BKM120 with RAD001, an mTORC1 inhibitor that penetrates the BBB[7,8].

Whereas DF-BM355 PDXs showed limited response to the combination of lapatinib and RAD001 (**Supplementary Fig. 2e**), the administration of BKM120 and RAD001 together resulted in marked tumor regression, as measured by bioluminescence (**Fig. 2a**). Owing to the unprecedented nature of this response, we removed two mice from the control group bearing large tumors, and introduced BKM120 and RAD001. The large tumors also regressed over time (**Fig. 2a**). Magnetic resonance imaging (MRI) before and after treatment confirmed these results (**Fig. 2b**). The remaining mice in the control group quickly reached the study endpoint (developing systemic

[1]Department of Cancer Biology, Dana-Farber Cancer Institute, Boston, Massachusetts, USA. [2]Department of Biological Chemistry and Molecular Pharmacology, Harvard Medical School, Boston, Massachusetts, USA. [3]Department of Medical Oncology, Dana-Farber Cancer Institute, Harvard Medical School, Boston, Massachusetts, USA. [4]Department of Pathology, Brigham and Women's Hospital, Boston, Massachusetts, USA. [5]Department of Biostatistics and Computational Biology, Dana-Farber Cancer Institute, Boston, Massachusetts, USA. [6]Lurie Family Imaging Center, Dana-Farber Cancer Institute, Boston, Massachusetts, USA. [7]Department of Neurosurgery, Brigham and Women's Hospital, Boston, Massachusetts, USA. [8]School of Public Health, Yale University, New Haven, Connecticut, USA. [9]Department of Radiation Oncology, Dana-Farber Cancer Institute, Boston, Massachusetts, USA. [10]Department of Radiation Oncology, Brigham and Women's Hospital, Boston, Massachusetts, USA. [11]These authors contributed equally to this work. [12]These authors jointly directed this work. Correspondence should be addressed to J.J.Z. (jean_zhao@dfci.harvard.edu), K.L.L. (keith_ligon@dfci.harvard.edu), and N.U.L. (nancy_lin@dfci.harvard.edu).

Figure 1 Establishment of orthotopic HER2-positive BCBM PDXs. (**a**) Schematic depicting the process of generating orthotopic PDX BCBM models for use in preclinical studies. Fresh brain metastatic tissues from individuals with BCBM were grafted directly into the brains of female SCID mice. The xenografts in the brain were explanted, dissociated and transduced with a luciferase gene, and then re-injected into new cohorts of mice. P0, primary graft; P1–P5, passage number in mice. Scale bars, 5 cm (left); 500 μm (middle). (**b**) Representative histologic and immunophenotypic analyses of two patient surgical biopsies and the corresponding PDXs. Scale bars, 25 μm. (**c**) Compiled result of PTEN immunohistochemistry (IHC) scores performed on 27 human HER2-positive BCBM samples. 0, no staining in >90% of tumor cells; 1+, weak staining in >75% of tumor cells; 2+, strong staining in >75% of tumor cells.
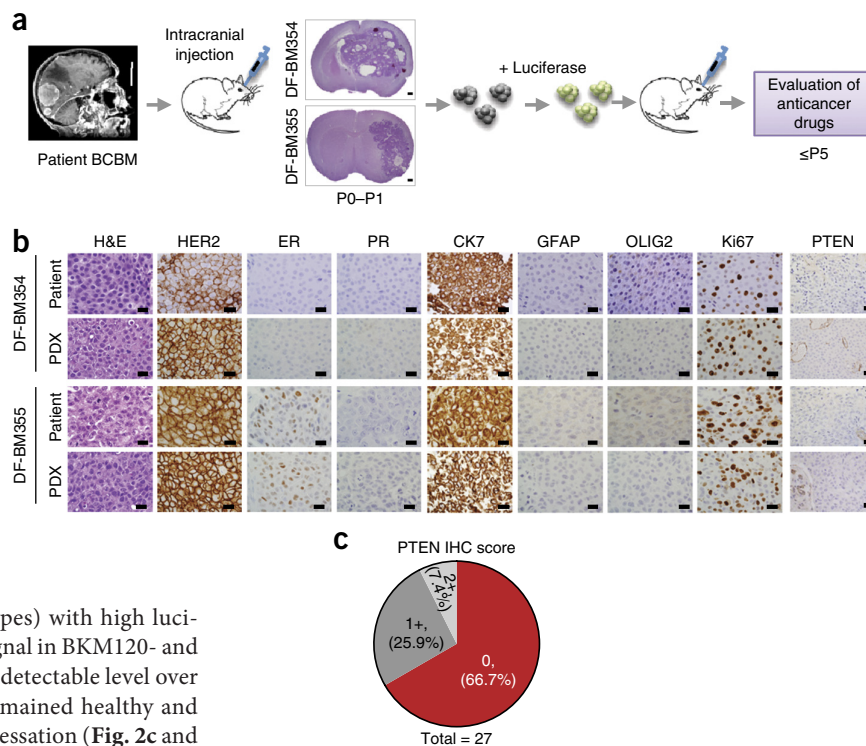
symptoms of morbidity or neurologic phenotypes) with high luciferase signals (**Fig. 2c**). Notably, the luciferase signal in BKM120- and RAD001-treated tumors declined to a nearly undetectable level over the treatment period of 14 weeks, and mice remained healthy and luciferase-signal-free for weeks after treatment cessation (**Fig. 2c** and **Supplementary Fig. 2e**). All mice treated survived the 210-d period of observation, whereas all mice in the control group died after approximately 90 d (**Fig. 2d**). To avoid potential confounding symptoms from aging-associated disease phenotypes, we stopped treatment around 210 d, at which point the recipient mice were 270–280 d old.

The unique efficacy of this combination is underscored by results from additional experiments; neither a combination of BKM120 with the MEK inhibitor MEK162—chosen because of high p-ERK levels in the PDX tumors—nor a combination of BKM120 with the BET bromodomain inhibitor JQ1, which downregulates MYC expression—chosen owing to *MYC* amplifications in the PDX tumors—showed efficacy (**Supplementary Figs. 3** and **4**).

To understand the mechanism underlying the synergy between BKM120 and RAD001, we harvested tumors from mice after 4 d of treatment for pharmacodynamic assessment. Although both monotherapies reduced p-S6RP, as compared to control, neither drug alone significantly suppressed p-4EBP1 (**Fig. 2e**), which suggests that mTORC1 was not completely inhibited. These observations are consistent with reports indicating that although rapamycin (an mTORC1 inhibitor) stably inhibits p-S6RP, its effect on p-4EBP1 is short lived, and that a rapid re-emergence of p-4EBP1 contributes to rapamycin resistance[9]. Notably, combined BKM120–RAD001 treatment markedly reduced p-4EBP1 and also significantly decreased proliferation (as measured by Ki67 staining), and increased apoptosis (cleaved caspase-3 staining), relative to monotherapies and the control (**Fig. 2e**).

To determine whether these results could be replicated in other BCBMs, we tested the same therapy in the remaining four PDX models of BCBM (DF-BM354, DF-BM463, DF-BM507 and DF-BM590). Consistently with our findings in DF-BM355, neither BKM120 nor RAD001 monotherapy had meaningful effects in the DF-BM354 model, whereas the combination therapy led to durable tumor regression, significant reductions in p-S6RP and p-4EBP1 and significant decreases in Ki67 staining, as compared to the control (**Fig. 2f** and **Supplementary Fig. 5a,b**). Notably, DF-BM354 and DF-BM355 show disparate ER statuses (**Fig. 1b**), which suggests that the BMK120–RAD001

combination might be effective for HER2-positive BCBMs, regardless of hormone-receptor expression. The DF-BM463 model also exhibited durable responses to BKM120–RAD001 therapy, along with similar changes in p-4EBP1, Ki67 and cleaved caspase-3 levels (**Fig. 2f** and **Supplementary Fig. 5c,d**).

By contrast, BKM120–RAD001 combination therapy had little effect on the survival of mice bearing DF-BM507 and DF-BM590 PDXs, and the amount of p-S6RP and p-4EBP1 was also not reduced in these models (**Fig. 2f** and **Supplementary Fig. 5e,f**). To understand the molecular basis for the differential therapeutic responses between models, we performed transcriptome analyses on tumors from untreated mice. The three responding models showed significantly higher expression of AKT–mTOR-dependent signature genes[10] than did two nonresponding models (**Fig. 2g**), which suggests that some, but not all, HER2-positive BCBMs depend on the AKT–mTOR pathway.

We also performed whole-exome sequencing (WES) of all five PDX tumors and matched samples from the donor patients' blood (patient blood was unavailable for DF-BM355). Copy-number variations (CNVs) were frequent in all five of the tumor models (**Supplementary Fig. 6**), and each PDX and its matched patient tumor shared almost identical CNVs (**Supplementary Fig. 7a**), suggesting conservation of genetic alterations in these PDXs. The rate of nonsynonymous somatic mutations in responding tumors was ~7–8 per Mb (**Fig. 2h**), in line with recently reported data that the mutation rate in HER2-positive BCBMs is roughly ten mutations per Mb[11]. The mutation rate in nonresponsive BCBMs, by contrast, was ~60–70 mutations per Mb (**Fig. 2h**). Relevant to this hypermutation phenotype is the knowledge that the two nonresponding PDXs were derived from patients who had more cycles of chemotherapy and/or radiation therapy than did the patients from whom the responding PDXs were derived (**Supplementary Table 2**). Hypermutation has been linked to mutations in DNA-repair genes[12], and indeed, therapy-resistant PDXs and their matched patient specimens harbored mutations
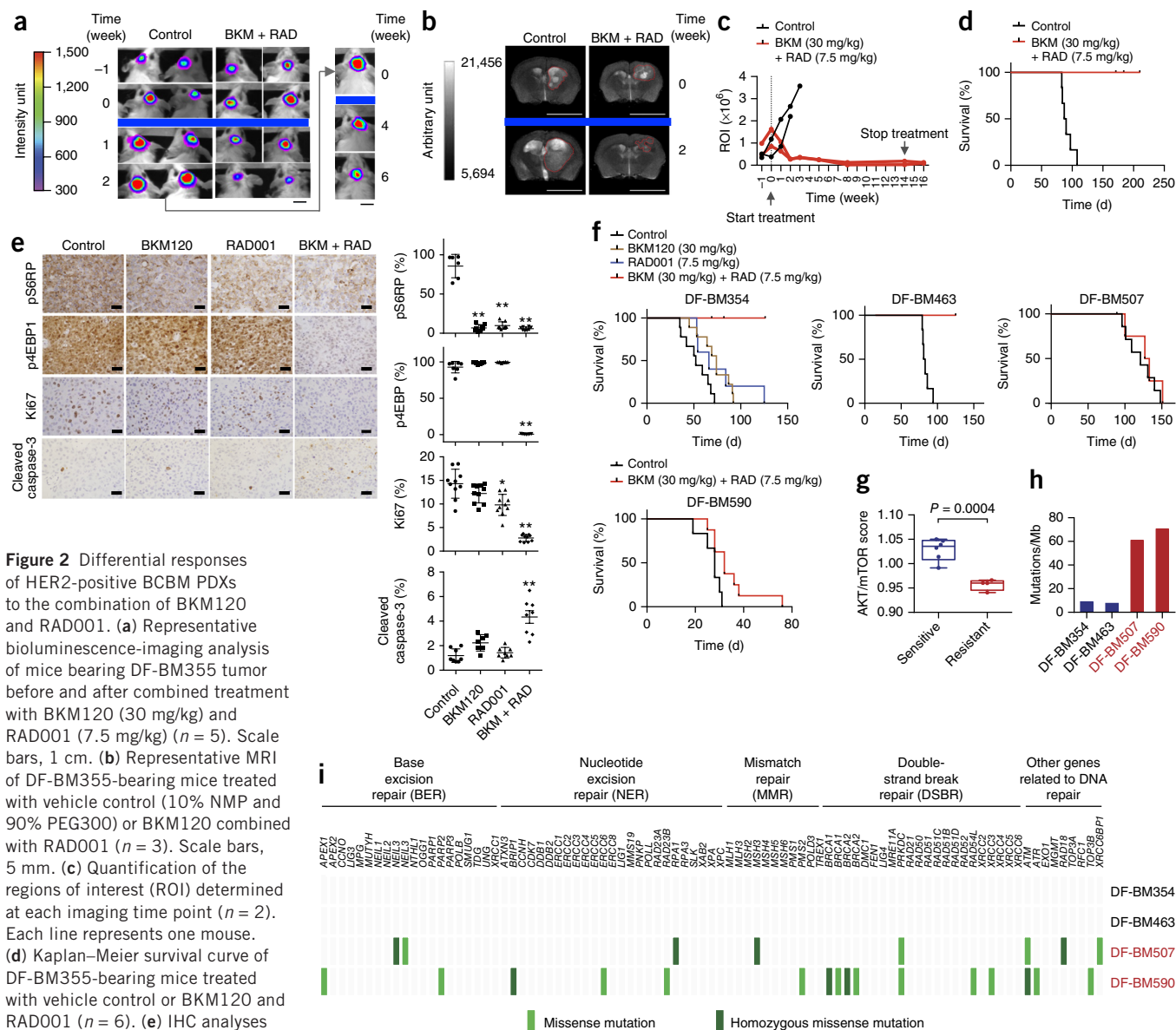
Figure 2 Differential responses of HER2-positive BCBM PDXs to the combination of BKM120 and RAD001. (**a**) Representative bioluminescence-imaging analysis of mice bearing DF-BM355 tumor before and after combined treatment with BKM120 (30 mg/kg) and RAD001 (7.5 mg/kg) ($n = 5$). Scale bars, 1 cm. (**b**) Representative MRI of DF-BM355-bearing mice treated with vehicle control (10% NMP and 90% PEG300) or BKM120 combined with RAD001 ($n = 3$). Scale bars, 5 mm. (**c**) Quantification of the regions of interest (ROI) determined at each imaging time point ($n = 2$). Each line represents one mouse. (**d**) Kaplan–Meier survival curve of DF-BM355-bearing mice treated with vehicle control or BKM120 and RAD001 ($n = 6$). (**e**) IHC analyses of p-4EBP1, p-S6RP, Ki67 and cleaved caspase-3 on DF-BM355 tumors treated for 4 d with indicated treatments. Scale bars, 25 μm. Error bars represent mean ± s.d. ($n = 6$–10 images per group). $*P < 0.05$, $**P < 0.01$, one-way analysis of variance (ANOVA), followed by Dunnett's test. (**f**) Kaplan–Meier survival curves of mice bearing DF-BM354, DF-BM463, DF-BM507 and DF-BM590 with vehicle control or compound, as indicated ($n = 5$–9). (**g**) Transcriptome analysis of AKT–mTOR-dependent signature genes from brain xenograft tumor tissues from untreated mice. Box plots correspond to the first and third quartiles, with upper and lower whiskers extending to the farthest value that is within 1.5× the interquartile range ($n = 4$–6 per group; $P = 0.0004$, Student's t test). (**h**) Number of somatic mutations in HER2-positive BCBM PDXs identified by WES. (**i**) Mutational profiling of a panel of DNA-repair genes.

in several DNA-repair genes (**Fig. 2i**, **Supplementary Fig. 7b** and **Supplementary Tables 3** and **4**). In agreement with this observation, a recent analysis of metastatic breast cancer samples from the BOLERO-2 trial revealed that high genomic instability is correlated with resistance to everolimus (RAD001)[13].

Given that the combination of BKM120 with RAD001 is already under clinical evaluation in advanced solid malignancies, the translation of our preclinical findings could be fast-tracked into the clinic for individuals with HER2-positive BCBM. More broadly, our study demonstrates that the use of brain-metastasis-specific PDX models facilitates the integration of phenotypic and genotypic analyses, and advances precision medicine for cancer.

METHODS

Methods and any associated references are available in the online version of the paper.

Accession codes. National Center for Biotechnology Information (NCBI) database of Genotypes and Phenotypes (dbGaP): WES data have been deposited under accession number phs001063.v1.p1. Gene Expression Omnibus (GEO): transcriptome data have been deposited under accession number GSE80722.

Note: Any Supplementary Information and Source Data files are available in the online version of the paper.

BRIEF COMMUNICATIONS

AUTHOR CONTRIBUTIONS

J.N., S.H.R., S.X., E.P.W., N.U.L., K.L.L. and J.J.Z. conceived and designed experiments. J.N., S.H.R., S.X., K.L.L. and J.J.Z. developed methodology. J.N., S.H.R., S.X., H.G., V.L., Y.J.K. and M.H. performed the surgeries and the *in vitro* and *in vivo* experiments. J.N., S.H.R., S.X., S.G., D.G.S., E.M., K.L.L. and J.J.Z. analyzed and interpreted data. J.N., S.H.R., S.X., S.G., J.D.I., I.E.K., G.-C.Y., T.M.R., E.P.W., N.U.L., K.L.L. and J.J.Z. wrote and/or revised the manuscript. J.N., S.H.R., S.X., L.A.R., Q.-D.N., A.H.L., R.D., E.B.C., B.M.A. and Z.C.W. provided administrative, technical or material support. H.G., V.L., Y.J.K. and M.H. provided technical assistance. E.P.W., N.U.L., K.L.L. and J.J.Z. supervised and coordinated all aspects of the work.

Reprints and permissions information is available online at http://www.nature.com/reprints/index.html.

1. Wikman, H. *et al. Breast Cancer Res.* **14**, R49 (2012).
2. Zhang, L. *et al. Nature* **527**, 100–104 (2015).
3. Filbin, M.G. *et al. Nat. Med.* **19**, 1518–1523 (2013).
4. Maire, C.L. *et al. Stem Cells* **32**, 313–326 (2014).
5. Thorpe, L.M., Yuzugullu, H. & Zhao, J.J. *Nat. Rev. Cancer* **15**, 7–24 (2015).
6. Elkabets, M. *et al. Sci. Transl. Med.* **5**, 196ra199 (2013).
7. Krueger, D.A. *et al. N. Engl. J. Med.* **363**, 1801–1811 (2010).
8. O'Reilly, T. *et al. Cancer Chemother. Pharmacol.* **65**, 625–639 (2010).
9. Choo, A.Y., Yoon, S.O., Kim, S.G., Roux, P.P. & Blenis, J. *Proc. Natl. Acad. Sci. USA* **105**, 17414–17419 (2008).
10. Creighton, C.J. *Oncogene* **26**, 4648–4655 (2007).
11. Brastianos, P.K. *et al. Cancer Discov.* **5**, 1164–1177 (2015).
12. Shlien, A. *et al.* Biallelic Mismatch Repair Deficiency Consortium. *Nat. Genet.* **47**, 257–262 (2015).
13. Hortobagyi, G.N. *et al. J. Clin. Oncol.* **34**, 419–426 (2016).

ONLINE METHODS

Patient-derived xenografts. Written informed consent was obtained from patients, and fresh brain metastases were acquired from patients with BCBMs undergoing neurosurgery at the Brigham and Women's Hospital as part of the Dana-Farber Institutional Review Board (IRB) approved protocol (DFCI IRB 93-085 and 10-417) within the Dana-Farber/Harvard Cancer Center (DF/HCC) Living Tissue Bank program. To establish patient-derived metastatic breast models, fresh tumor tissue was dissociated in gentleMACS C Tubes using mechanical and enzymatic methods (Miltenyi Biotech). A suspension of metastatic breast cells was prepared at a concentration of 100,000 viable cells per microliter, and temporarily incubated on ice before use in intracranial injections. 8–10-week-old female, severe combined immunodeficiency (SCID) mice acquired from Taconic (IcrTac:ICR-Prkdcscid) were anesthetized with oxygen-diluted isoflurane or ketamine and xylazine positioned into a stereotactic frame, whereby the head was secured by gentle pressure from ear bars while deep anesthesia was maintained. A 1-cm scalp incision was made to identify the bregma, which served as the zero coordinates ($x = 0$ mm, $y = 0$ mm, $z = 0$ mm). A burr hole was created in the skull in the right hemisphere at coordinates $x = 0$ mm, $y = 2$ mm, $z = 0$ mm, and each animal was injected with 100,000 viable tumor cells into the right striatum ($z = 2$ mm). The scalp was closed with 9-mm autoclips (BD Diagnostic Systems). Mice bearing xenografts were housed under standard conditions and monitored closely for the development of systemic symptoms of morbidity or neurologic phenotypes, including rapid body-weight loss, hunched posture, inability to obtain food or water or other humane endpoints necessitating euthanasia. After euthanasia, brain tumors from symptomatic animals were collected by dissection, dissociated and re-injected intracranially into additional animals (serial passaging *in vivo*). Luciferase expression was introduced into tumor cells from primary grafts (P0–1), and low-passage PDXs (at passage 5 or lower) were used for all therapeutic experiments. Alternatively, for neuropathological evaluation of brain tumors, euthanized animals bearing xenografts were perfused by intracardiac injection of 4% paraformaldehyde (PFA) in phosphate-buffered saline (PBS, pH 7.0), and the brain tissue samples with tumor lesions were processed by standard methods for paraffin embedding. H&E-stained sections were generated, and the tumors were then evaluated. All animal experiments were performed according to protocols approved by the Dana-Farber Cancer Institute Animal Care and Use Committee in compliance with NIH animal guidelines.

Immunohistochemistry. Diaminobenzidine (DAB), brightfield staining was performed, according to standard protocols using DAB EnVision+ System (Dako) on paraffin sections. Briefly, 5-μm-thick sections were deparaffinized with xylene, and this was followed by gradation washes in 100%, 95%, 80% ethyl alcohol before performing heat antigen retrieval in 10 mM sodium citrate buffer (pH 6.0) for 20 min. Subsequently, sections were treated with peroxidase block (Dako) for 10 min, and then incubated overnight at 4 °C with the following primary antibodies: PTEN (Cell Signaling #9559, 1:400), p-S6RP-Ser235/236 (Cell Signaling #2211, 1:400 or 1:1,000), p-4EBP1-Thr37/46 (Cell Signaling #2855, 1:400 or 1:1,000), cleaved caspase-3 (Cell Signaling #9664, 1:400), estrogen receptor (ER) (ThermoScientific SP1, 1:40), progesterone receptor (PR) (Dako PgR 636, 1:150), HER2 (ThermoScientific SP3, 1:50), CK7 (Dako, 1:100), GFAP (Dako #z0334, 1:500), OLIG2 (Chemicon #AB9610, 1:500) and Ki67 (Dako MIB-1,1:200 or Vector lab #VP K-451,1:1,000). After multiple washes with 1× Tris-buffered saline and Tween 20 (TBST) solution, slides were incubated at room temperature with corresponding species-specific horseradish peroxidase (HRP) conjugated secondary antibody from EnVision+ System (Dako) (100-μl pre made solution/slide) for 2 h or from Vector Laboratories (1:200) for 30 mins). Signal was visualized by the HRP–DAB reaction. Counterstaining for nuclei was performed using Mayer's hematoxylin stain, followed by graded dehydration and xylene washes. Coverslips were mounted with Permount (Fisher Scientific). Antibody validation is provided on the manufacturers' website.

Ki67 and cleaved caspase-3 indexes were calculated as a percentage of positive cells in four or five random areas of each sample. Images were captured at 40× or 60× magnification, and quantifications of Ki67 and cleaved caspase-3 immunoreactivity were performed using the Image J software with ImmunoRatio plugin. P-S6RP and p-4EBP indexes were calculated as a percentage of positive areas in

3–5 random areas of each sample. Images were captured at 40× or 60× magnification, and quantification of p-S6RP and p-4EBP immunoreactivity was performed using the Cellvigene software (VigeneTech). The IHC experiments and data analyses were done by two investigators blinded to the group allocation.

Lentiviral production and transduction. Human embryonic kidney (HEK) 293T cell line was obtained from the American Type Culture Collection (ATCC, Manassas, VA). The cells were maintained in DMEM supplemented with 10% FBS and 100 μg/ml penicillin–streptomycin. The cells were frozen after receipt and were used at early passages. No authentication or mycoplasma-contamination test was done. The pLenti-blasticidin-Luciferase vector was co-transfected with pCMV-delta8.9 and pMD.G at the ratio of 4:3:1 into HEK293T cells by PEI (1 μg/μl) (4:1 to DNA). The culture medium was replaced 1 d after transfection, and the viral supernatants were collected 1 d and 2 d later. The viral supernatants were filtered through a 0.45-μm filter and were then concentrated by ultracentrifugation (SW28, 16,600 rpm, 2 h). Viral pellets were resuspended in PBS and aliquoted and stored at −80 °C for future use. Viral titers were determined by qPCR Lentivirus titration Kit (Applied Biological Materials, Inc.)

Tumor cells were isolated from passage 0 or 1 PDXs and transduced with a lentivirus encoding Luciferase (pLenti-blasticidin-Luciferase) at ~MOI 5 in suspension overnight with polybrene 8 μg/ml, and then subjected to 3-d antibiotic selection with blasticidin 2 μg/ml to enrich the population of blasticidin-Luciferase expressing cells in NeuroCult NS-A media (Stemcell Technologies) supplemented with heparin sulfate (2 mg/ml), epidermal growth factor (EGF, 20 ng/ml), basic fibroblast growth factor (bFGF, 20 ng/ml), and hydrocortisone (0.5 μg/ml). These tumor cells were then propagated in mice.

Bioluminescence imaging. For imaging, mice were injected i.p. with D-luciferin (Promega) (~60 mg/kg), together with anesthetized reagents ketamine (100 mg/kg) and xylazine (7 mg/kg). 10 min later, luciferase expression was recorded and images were obtained with Kodak Image Station 4000MM for 20 min (DF-BM355) or 5 min (DF-BM354). The signals were analyzed with CareStream MI Software.

Treatment *in vivo*. BKM120 was dissolved in 10% NMP with 90% PEG300 and given orally once per day at 30 mg/kg. RAD001 was freshly prepared from a micro-emulsion pre-concentrate (Novartis) with 5% glucose dilution, or dissolved in 10% NMP with 90% PEG300, and delivered orally each day to mice at 7.5 mg/kg. Lapatinib was dissolved in 0.5% hydroxypropyl methylcellulose (HPMC) with 0.1% Tween80 and administered at 100 mg/kg body weight once a day by oral gavage. All compounds were purchased from Haoyuan ChemExpress, Co.

Treatment was started at 3–6 weeks after the injection of tumor cells, once mice developed luciferase signals with ROI 0.2–$1.0 × 10^6$ as baseline levels of tumor lesion. Tumor-bearing mice were randomized into control and treatment groups, and five or six mice were used for each experimental cohort. Mice were followed to their endpoints (30–100 d) or, if treated mice survived longer than the mice in the control groups, to a point 50–100% longer than the endpoints of the control mice. The sample size for the experiments was determined by the pilot studies in the laboratories and the StatsToDo program on the basis of the probability of type 1 error (α) at 0.05, power at 0.8, expected difference between two means, and s.d. within the group. The drug treatments with the outcome measurements and the data analysis were done by two investigators blinded to the group allocations.

MRI imaging. MRI experiments were performed on a Bruker BioSpec 7.0 Tesla 30 cm clear bore USR (Ultra Shielded Refrigerated) horizontal bore Superconducting Magnet System, equipped with the B-GA12S2 gradient and integrated with up to second-order room-temperature shim system, which provides a maximum gradient amplitude of 440 mT/m and a slew rate of 3440 T/m/s. The Bruker-made 23-mm ID birdcage volume radiofrequency (RF) coil was used for both RF excitation and receiving. AutoPac with laser was used for precise animal positioning. Animals were anesthetized throughout the imaging procedure through the inhalation of a mixture of 1.5% isoflurane into medically supplied air. Animal respiration and temperature were monitored and regulated by the SAII (Stony Brook, NY) monitoring and gating-system model 1025T.

Bruker Paravision 5.1 was used for MRI data acquisition. Once animals were positioned in the magnet, a three orthogonal scout imaging protocol was loaded and run with the traffic light, which enabled it to run the automatic center frequency, automatic shim, reference RF gain, receive gain and then acquire the reference images. T2 weighted images were obtained from fast spin echo (RARE) with fat suppression sequence and the following parameters: TE (echo time) = 33 ms; TR (repetition time) = 2500 ms; rare factor = 8; number of averages = 2; total acquisition time = 2 min 40 s; FOV (field of view) = 20×20 mm^2; matrix size = 256×256; spatial resolution = 78×78 µm^2; slice thickness = 1.0 mm; and number of slices = 12. 3D volume reconstructions were obtained using OsiriX software.

Whole-exome sequencing. The exome was sequenced on the Ion Torrent Proton platform (Life Technologies, Thermo Fisher), according to the manufacturer's instructions. Briefly, genomic DNA was extracted from the patient's peripheral blood or PDX tumors using DNeasy blood & tissue kit (Qiagen). DNA libraries were constructed from 100 ng of gDNA using the Ion AmpliSeq Exome kit (Life Technologies, Thermo Fisher) that provides targeted regions of greater than 97% of the coding exons of the human genome. The final exome libraries were quantitated by Ion Library Quantitation Kit (Life Technologies, Thermo Fisher). Two or three libraries were multiplexed and clonally amplified to obtain template-positive ion-sphere particles by using the Ion OneTouch 2 System (Life Technologies, Thermo Fisher), and were then sequenced on an Ion Torrent Proton using one PI chip kit V2 (Life Technologies, Thermo Fisher). The alignment of sequencing reads was performed using Torrent Suite Software and Torrent Server. Further data analysis, variant calling and the annotation of variants were carried out by AmpliSeq Exome single-sample (Somatic) workflow and tumor–normal pair workflow by using ion reporter software (Life Technologies, Thermo Fisher). Variant calls with fewer than ten reads for normal samples and 20 reads for tumor samples were removed. For the analyses of somatic mutations of DNA-repair genes in the tumors, mutation calls with fewer than 20 reads were excluded. R and Bioconductor packages[14] were used to prioritize and visualize the sequencing data. The segment-plotting tool from the read-Depth package for R was further modified to visualize CNV alterations[15]. The sequencing data have been deposited in the NCBI dbGaP with the accession number phs001063.v1.p1.

Transcriptome analysis. AmpliSeq human-transcriptome libraries were constructed and sequenced in technical duplicate using the Ion Proton platform, according to the manufacturer's instructions and as previously described[16]. Briefly, 10 ng of total RNA samples from brain xenograft tumor tissue was used for cDNA library preparation. Eight libraries were multiplexed and clonally amplified by using the Ion OneTouch 2 System (Life Technologies, Thermo Fisher), and then sequenced on an Ion Torrent Proton machine. Data was first analyzed by Torrent Suite and ampliSeqRNA analysis plugin (Life Technologies, Thermo Fisher) to generate count data. Count data were transformed using the R-bioconductor packages DESeq2 (ref. 17), then log$_2$ transformed and mean-normalized by gene to enable comparison. Given that the two agents in this study target the PI3K–AKT–mTOR pathway, we searched MSigDB (http://software.broadinstitute.org/gsea/msigdb) for gene expression signatures representing this pathway using the terms 'AKT AND mTOR.' Of the results, only one signature was experimentally derived[10]. We reviewed the primary manuscript and used the 35 'up' genes in the original manuscript as the 'AKT–mTOR' signature. The AKT–mTOR signature score represents the mean of the 35 upregulated genes induced by AKT in a transgenic mouse model and sensitive to mammalian (or mechanistic) target of rapamycin (mTOR) inhibitor RAD001 in a previously published study (*AKT1, BIK, BSG, DDR1, CDC34, CLDN3, CYB561, GPX4, HNRPAB, LASP1, MMP15, MVK, NEDD8, NEU1, PCTK1, POR, PRKCD, PVRL2, SPINT1, UBE2M, TMED10, DUSP10, CLSTN1, PMPCA, BRMS1, TJP3, ARHGEF16, ADIPOR1, SLC37A1, KCTD5, TOLLIP, SYNJ2BP, RNF126, CORO1B*)[10]. Box plots correspond to the first and third quartiles (the 25th and 75th percentiles) with upper and lower whisker extending to the farthest value that is within 1.5× of the interquartile range. Code is available upon request. The transcriptome data have been deposited in the NCBI GEO with the accession number GSE80722.

Statistical analysis. Statistical significance was determined using unpaired Student's *t* test or ANOVA by GraphPad Prism 6 (GraphPad Software). Data are considered to be significant when *P* values are <0.05. Sample sizes and animal numbers were chosen on the basis of power calculations of 0.8 and pilot studies performed in the laboratory. No animals were excluded from the analysis.

14. Gentleman, R.C. *et al. Genome Biol.* **5**, R80 (2004).
15. Miller, C.A., Hampton, O., Coarfa, C. & Milosavljevic, A. *PLoS One* **6**, e16327 (2011).
16. Wang, Y. *et al. Cell* **163**, 174–186 (2015).
17. Love, M.I., Huber, W. & Anders, S. *Genome Biol.* **15**, 550 (2014).